RAA 2021 Vol. **21** No. **5**, 116(8pp) doi: 10.1088/1674-4527/21/5/116

http://www.raa-journal.org *http://iopscience.iop.org/raa*

Research in Astronomy and Astrophysics

Ground experiments and performance evaluation of the Low-Frequency Radio Spectrometer onboard the lander of Chang'e-4 mission

Xin-Ying Zhu[1], Yan Su[1,3], Yi-Cai Ji[2,3], Hong-Bo Zhang[1,3], Bo Zhao[2], Jun-duo Li[1], Shun Dai[1], Xi-Ping Xue[1] and Chun-Lai Li[1,3]

[1] Key Laboratory of Lunar and Deep Space Exploration, National Astronomical Observatories, Chinese Academy of Sciences, Beijing 100101, China; *suyan@bao.ac.cn*
[2] Institute of Electronics, Chinese Academy of Sciences, Beijing 100190, China; *ycji@mail.ie.ac.cn*
[3] University of Chinese Academy of Sciences, Beijing 100049, China

Received 2019 October 29; accepted 2020 December 7

Abstract The Low-Frequency Radio Spectrometer (LFRS) is a scientific payload onboard the Chang'e-4 lunar lander launched in December 2018. The LFRS provides in-situ measurements of the low-frequency radio phenomena on the far-side of the Moon for the first time in human history. To evaluate the performance of the LFRS, a series of ground experiments are conducted using an engineering model of the LFRS. It is not easy to perform the experiments because the Electro Magnetic Interference (EMI) from the Chang'e-4 lunar lander itself and the environment is very intense. The results after EMI mitigation show that the sensitivity of the LFRS may be 10^{-18}W m^{-2} Hz^{-1}.

Key words: Moon: far-side — space vehicles: instruments — techniques: spectroscopic

1 INTRODUCTION

The atmosphere is not perfectly transparent at any radio frequency. Radio waves are scattered and absorbed by Earth's atmosphere. Low-frequency astronomical observation from the ground is limited by severe ionospheric distortions below 50MHz and complete reflection of radio waves below 10–30 MHz (Jester & Falcke 2009). Even from an orbiter around the Earth, human-made interference from the Earth and natural radio emission from the Sun turn out to be too overwhelming for any observations in this frequency range. For these reasons, the low-frequency end is indeed one of the last portions of the electromagnetic spectrum to remain terra incognita in astrophysics (Boonstra et al. 2010; Bentum et al. 2011; Jester & Falcke 2009; Takahashi 2003; Wolt et al. 2012).

Chang'e-4 probe is the first mission landed on the far-side of the Moon in human history. The probe was launched at 18:23 (UTC) on 2018 December 7, and landed successfully in the Von Kármán crater within the South Pole-Aitken (SPA) basin at 2:26 (UTC) on 2019 January 3. It will attempt to collect new evidence from the most massive crater in the solar system to determine the age and composition of an unexplored region of the Moon, as well as develop technologies required for the later stages of the program (Li et al. 2019; Wu et al. 2017, 2019). The Low-Frequency Radio Spectrometer (LFRS) is a scientific payload onboard the Chang'e-4 lunar lander. The primary motivation for the LFRS is to learn about the universe through low-frequency spectral window. The Moon can be utilized as a shield against unwanted radiations from the Earth. By taking advantage of the unique environment, many astrophysical topics of interest such as cosmology with HI line emission, solar and planetary radio bursts, local plasma environment above the Moon's surface, ultra-high energy particle detection, meteoritic impacts could be studied through low-frequency observations (Jester & Falcke 2009; Lazio et al. 2011; Wolt et al. 2012). According to the characteristics of the Chang'e-4 mission, the main scientific objectives of the LFRS are to probe solar radio bursts and local plasma environment above the Moon's surface in the frequency range 0.1–40MHz.

The Chang'e-4 probe was initially built as a backup for Chang'e-3 and became operational after Chang'e-3 successfully landing in 2013. According to Electro Magnetic Compatibility (EMC) test results of Chang'e-4, the Electro Magnetic Interference (EMI) from the Chang'e-4 lunar lander itself is very intense, so all target radio emissions are hidden in the EMI noise. A method is proposed in order to suppress the significant interference

Table 1 Specifications of the LFRS Instrument

No.	Parameter	Characteristic
1	Frequency	0.1–40 MHz
2	Receiver sensitivity	$\leq 10\text{nV}/\sqrt{\text{Hz}}$
3	Dynamic Range	≥ 75 dB
4	Frequency Resolution	≤ 10 kHz (0.1–2.0 MHz) ≤ 200 kHz (1.0–40 MHz)
5	Max allowed bit rate	5 Mbps
6	Power	≤ 24 W

from the lander. Experiments on the ground (On Earth) are an essential tool for evaluating the payload performance, so a series of ground experiments were performed for this reason. In addition, the EMI mitigation method was also verified during the ground experiments.

2 INSTRUMENT DESCRIPTION

The LFRS which is mounted on the top of the Chang'e-4 Lander, was designed by Institute of Electronics, Chinese Academy of Sciences (IECAS) together with National Astronomical Observatories, Chinese Academy of Sciences (NAOC), and manufactured by IECAS. The actual working environment of the LFRS on the Moon is shown in Figure 1. This picture was taken by the Chang'e-4 cruiser.

The LFRS consists of sensors, pre-amplifiers, electronics unit and cable assemblies. The sensors and pre-amplifiers are installed outside the lander cabin, while the electronics unit is installed inside. The sensors are three 5-meter-long antennas which are mounted on the top of the lander orthogonally (Arts et al. 2010). Another 20 cm long antenna is mounted near the root of the long antenna as an auxiliary reference antenna. The signals of the above four antennas are pre-amplified and fed to the electronics unit. The electronics unit includes a control unit, a four-channel radio receiver covering the full band of 0.1−40MHz, and a calibration unit, etc (Ji et al. 2017).

The three 5-meter-long antennas receive both the scientific radio signals and the EMI of the lander, while the 20 cm long antennas only receive the EMI of the lander. The data of the 20 cm long antennas will be used to suppress the EMI in the off-line data processing stage. The specifications of the LFRS are summarized in Table 1.

3 GROUND EXPERIMENT

The main purposes of the ground experiments were to evaluate the performance of the prototype model of the LFRS and verify the off-line data processing method. According to the EMC test results of the Chang'e-4 lander, the detection capability of the LFRS is related to its technical performance and depends on the EMI mitigation method for noise suppression of the lander. Therefore, the EMI mitigation method is also tested in the ground experiments.

3.1 Experimental Setup

The engineering model which is identical, in form, fit and function to the flight model, was tested in the ground experiments. The experimental settings are shown in Figure 2. The EMI from the Chang'e-4 lunar lander was simulated by an arbitrary waveform generator which reproduced the lander noise recorded during the EMC test. Both the sinusoidal and wide-band signals generated by a vector signal generator were used to emulate the sky signals. The format of the emulated sky signals is listed in Table 2.

3.2 Experimental Method

As can be seen in Table 2, nine experiments were performed. Different rows in Table 2 mean different configurations of the emulated sky signal. Each configuration should be verified by an experiment. Each experiment was done in two steps. First, the signals were recorded by the LFRS while the simulated noise was off. Next, the simulated noise was turned on, both the simulated noise and the emulated sky signal were recorded by the LFRS.

A method named adaptive interference cancellation is used to suppress the EMI from the lander (Fridman & Baan 2001). A separate, dedicated reference channel is designed in order to obtain an independent estimate of the EMI from lander. The 20 cm long antenna for the reference channel is installed very close to the lander, near the root of the 5-meter-long antenna, as shown in Figure 2. The received signal from the short antenna is almost the EMI from the lander, because of the limited sensitivity for external signals. The signals received by the 5 meter long antenna, are be corrected using the signals received by the short reference antenna to suppress the EMI from the lander, the emulated sky signals with EMI and without EMI are compared to evaluate EMI mitigation. For the data of every experiment, the first 50 groups of data are averaged as correction coefficient. For every subsequent signal received by the antenna with a length of 5 meter is corrected using the corresponding signal received by the short reference antenna and the estimated correction coefficient. 75 groups of data (about 5 minutes) are averaged as the result of the experiments. The above method we used to suppress the EMI from the lander is

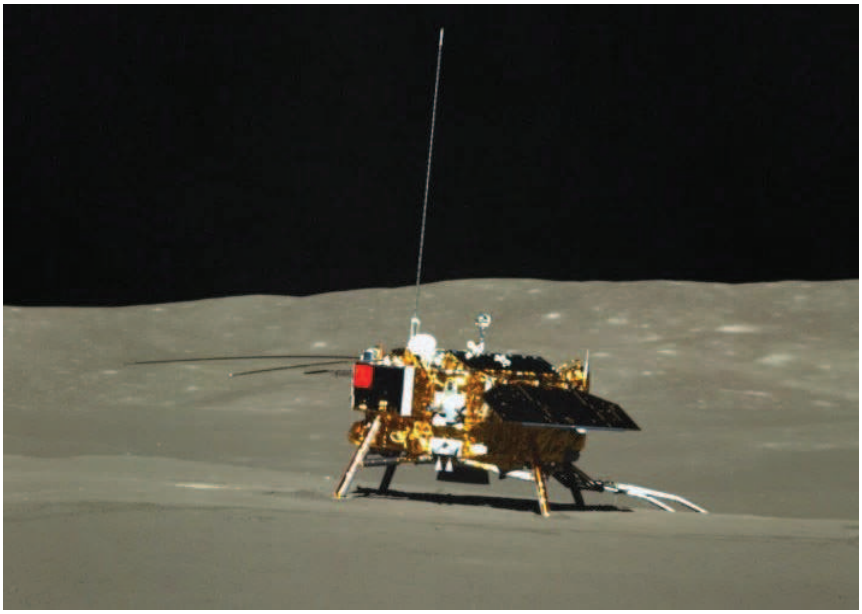

Fig. 1 The actual working environment of the LFRS on the Moon. This photo was taken by the Chang'e-4 cruiser.

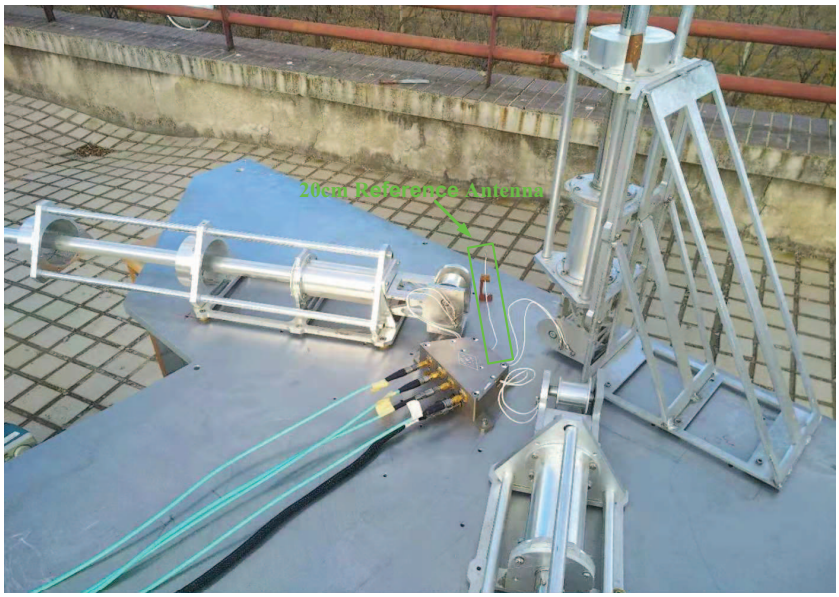

Fig. 2 Photograph of the LFRS antennas and the pre-amplifier.

shown in Equation (1).

$$
\begin{aligned}
&C_{\,a}\,(f) = \frac{\sum\limits_{i=1}^{50} U_{\,i}^{\,a}\,(f)}{\sum\limits_{i=1}^{50} U_{\,i}^{\,d}\,(f)},\\
&UC_{\,50+j}^{\,a}\,(f) = U_{\,50+j}^{\,a}\,(f) - C_{\,a}\,(f) \times U_{\,50+j}^{\,d}\,(f),\\
&UO^{\,a}\,(f) = \tfrac{1}{75}\sum_{j=1}^{75} UC_{\,50+j}^{\,a}(f),
\end{aligned}
\tag{1}
$$

where $U_{\,i}^{\,a}\,(f)$ is the ith group data output by LFRS which is an amplitude spectrum array of 5-meter-long antenna a, $U_{\,i}^{\,d}\,(f)$ is the ith group data of reference antenna d, $C_{\,a}\,(f)$ is the array of correction coefficient of antenna a, $UC_{\,50+j}^{\,a}\,(f)$ is the $50+j$th group of amplitude spectrum array which is corrected by reference antenna data and the array of correction coefficient, $UO^{\,a}\,(f)$ represents the final amplitude spectrum array of 5-meter-long antenna a.

The advantage of adaptive interference cancellation lies in keeping the structure of the signal-of-interest intact, the subtraction of an EMI estimate should not affect the wanted radio signal. This kind of EMI cancellation is especially useful for the LFRS observations where

Table 2 Format of the Emulated Sky Signals

No.	Signal Mode	Frequency	Amplitude	Remark
1	Sinusoidal signals	1.8 MHz	24 dBm	Sinusoidal signals are generated by arbitrary waveform generator
2		5 MHz	18 dBm	
3		8 MHz	18 dBm	
4		10 MHz	4 dBm	
5		22.5 MHz	–8 dBm	
6		38 MHz	–8 dBm	
7	Wide-band signals	1.75 MHz	20 dBm	Bandwidth:100kHz generated by vector signal generator
8		5 MHz	20 dBm	Bandwidth:1MHz generated by vector signal generator
9		20 MHz	20 dBm	Bandwidth:1MHz generated by vector signal generator

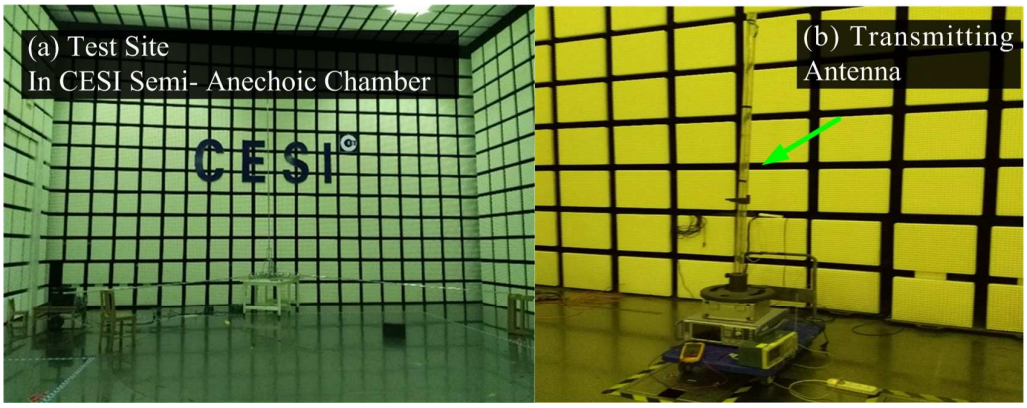

Fig. 3 Photographs of the test site CESI semi anechoic chamber.

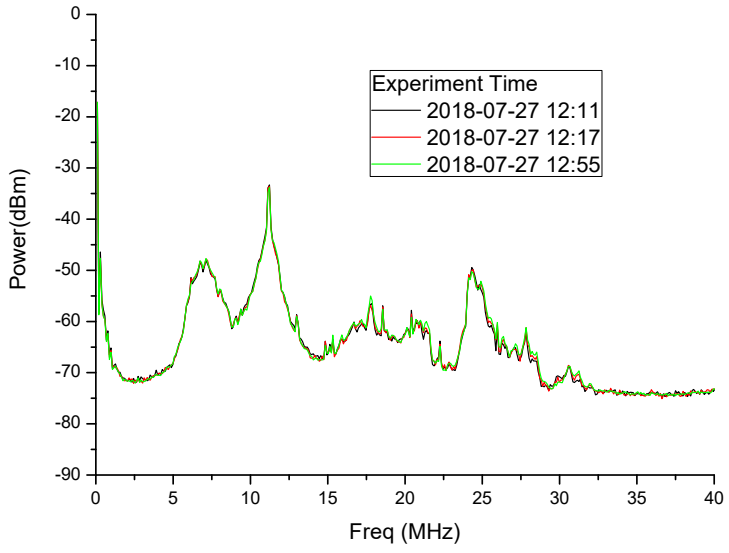

Fig. 4 Background signal spectra on site CESI semi-anechoic chamber.

the EMI and the signal-of-interest occupy the same frequency domain, but the effectiveness of the method also depends on the temporal stability of correction coefficient. Equation (1) is workable under the assumption of constant correction coefficient during the later averaging. Furthermore, the effectiveness of this adaptive interference cancellation also depends on the sensitivity of the reference channel. There will be a loss of signal-of-interest after processing, if the auxiliary reference is sensitive enough to receive the external signals.

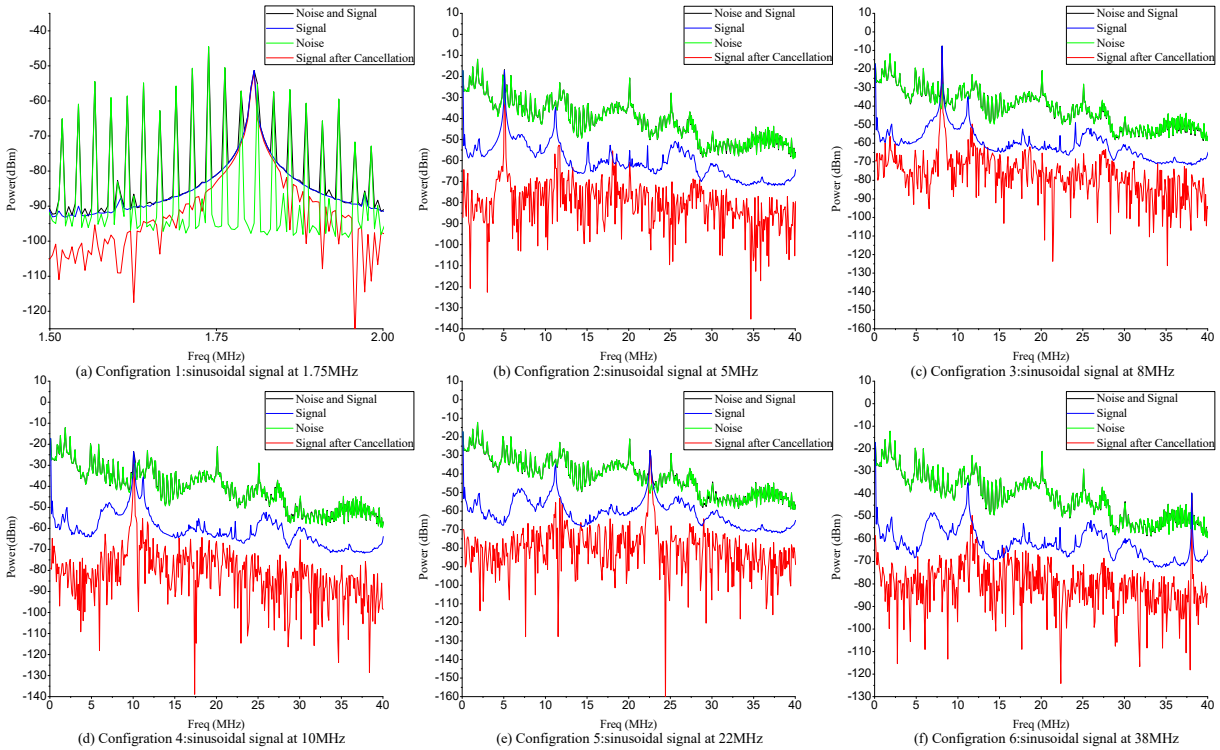

Fig. 5 Typical results of sinusoidal signals tests.

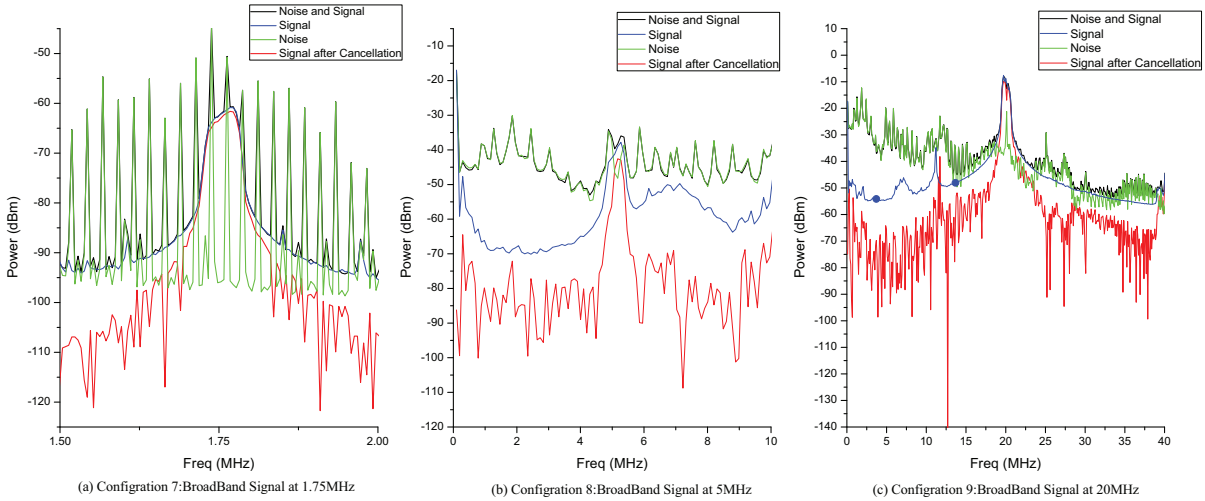

Fig. 6 Typical results of broadband signals tests.

3.3 Experimental Procedure

In order to prevent the low-frequency RFI from environment and simulate an open area test site, a semi-anechoic chamber located in China Electronic standardization Institute (CESI) was selected as the site of the ground experiments as shown in Figure 3(a)-(b). The semi-anechoic chamber consists of a 23m(Length)$\times$ 14 m(Width)$\times$ 9 m(Height) shielded enclosure. The chamber is lined with hybrid absorbers (model number IP-130BLB) which consist of carbon loaded polystyrene foam absorber bonded to the ferrite absorber backing. The guaranteed level of shielding effectiveness in the chamber would provide over the frequency range of 100 kHz to 18 GHz is 100 dB. Due to good electromagnetic shielding effectiveness of the semi-anechoic chamber, desired results of the ground experiments were achieved. The results and performance analysis are presented in the following section.

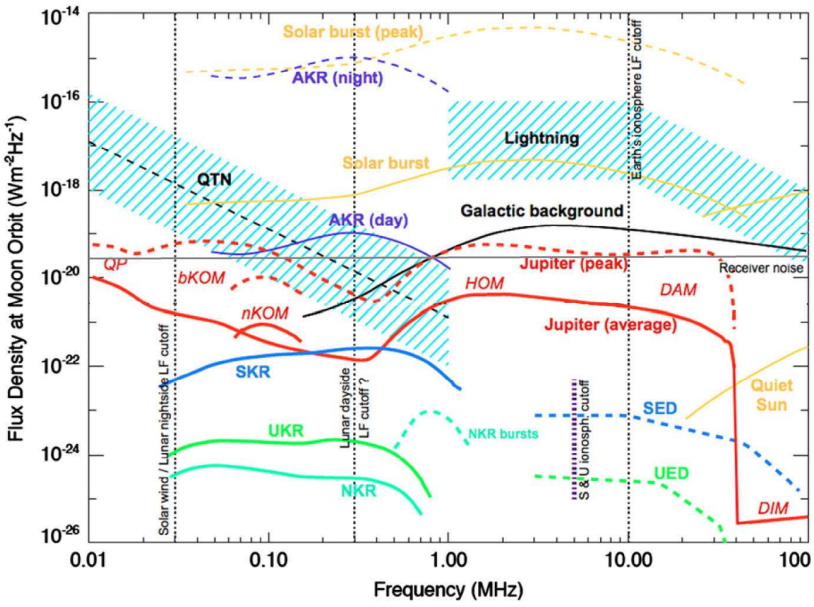

Fig. 7 Average and peak spectra of the various planetary magnetosphere and atmospheric radio components (Zarka et al. 2012).

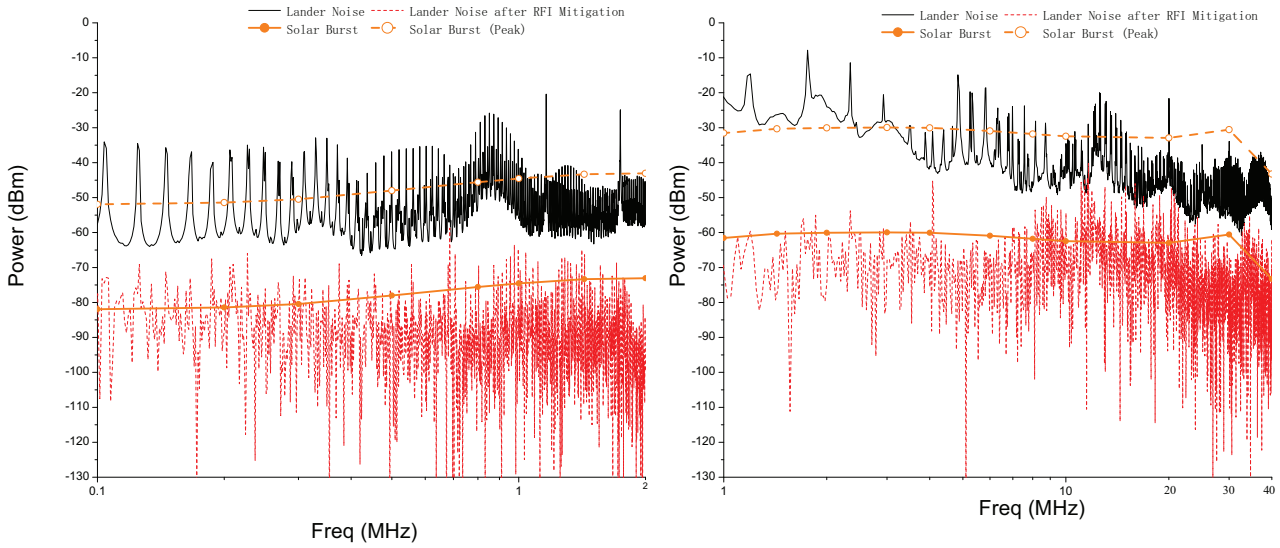

(a) Frequency range :0.1~2MHz RBW:1.22kHz

(b) Frequency range :1~40MHz RBW:24.42kHz

Fig. 8 Power spectrum received by the LFRS on the Moon caused by the solar burst and lander noise.

4 RESULTS AND PERFORMANCE ANALYSIS

4.1 Results

At the beginning of the experiment, the background noise of the site was tested. Figure 4 shows the background signal spectra received by the LFRS's 5-meter-long antenna in the semi-anechoic chamber. The Y-axis represents the amplitude of the signal spectrum in dBm, while the X-axis shows the frequency of the signal spectrum in MHz. Three tests were performed to check the characteristics of the background signals (black, red and green lines in Fig. 4). As you can see by Figure 4, although there are still RFI from the computers, test instruments, power supply, etc., the power and frequency of the RFI do not appreciably change over observable time. For the above

the reasons, the results from the experiments in the semi-anechoic chamber are used for analysis and performance evaluation of the LFRS.

Figure 5 shows the typical results of sinusoidal signals tests. According to the configuration of Table 2, six tests of sinusoidal signals mode were carried out. The method that is briefly described in Section 3.2 was used for EMI mitigation. In Figure 5 the blue lines indicate the spectrum of the generated signal described in Table 2. The green lines show the spectra of lander noise recorded during the EMC test. The black lines represent mixed spectra of signal and lander noise. The red lines reflect the spectra after EMI mitigation. The position of the red line relative to the position of the black line could be used to see the effectiveness of EMI mitigation. As shown in Figure 5, about 20 to 40 dB noise reduction could be received 0.1–40 MHz after EMI mitigation, while the sinusoidal signals are not severely distorted.

Figure 6 show the typical results of broadband signal tests. As shown in Figure 6, about 20 to 40 dB noise reduction could be received in 0.1–40 MHz after EMI mitigation, while the broadband signals are not severely distorted.

4.2 Performance Analysis

Average and peak spectra of the various planetary magnetosphere and atmospheric radio components as they would be measured from the Moon surface or orbit are displayed in Figure 7. As stated in Section 1, the primary scientific objective of the LFRS is to probe radio emission from the solar burst on the surface of the Moon, so the performance analysis focus on the average and peak spectra of the solar burst.

Because of the existence of lander noise, the detection capability of the LFRS is not only related to its technical performance, but also depends on the EMI mitigation method for the lander's noise suppression. In order to analyse the performance, the power of the signal received by the LFRS on the Moon caused by the solar burst and lander noise are estimated and compared in Figure 8.

The power of the signal from the solar burst (yellow lines in Fig. 8) could be estimated by solar burst flux density (solid or dashed yellow line in Fig. 7) and the LFRS technical parameters using the Equation (2), where E is the electric field strength that produces voltage at the terminal of the antenna, S is the flux density in W m^{-2} Hz^{-1} of the wave, η is the intrinsic impedance of free space, B is the bandwidth of the LFRS, U_a is the voltage at the terminal of the LFRS's antenna, h_e is the effective length of the antenna, U_{preamp} is the voltage outputted by pre-amplifier, Z_a is the impedance of the LFRS's antenna, Z_{preamp} is the impedance of the LFRS's pre-amplifier, G_{preamp} is the gain of the LFRS's pre-amplifier, P_{out} is the output power of the LFRS's receiver, G_{rec} is the gain of the LFRS's receiver, L_{line} is the insert loss of the cable between the pre-amplifier and the receiver, Z_L is the load resistance of the receiver.

$$\begin{aligned} E &= \sqrt{2\eta BS} \\ U_a &= E \times h_e \\ U_{\mathrm{preamp}} &= \frac{U_a Z_{\mathrm{preamp}} G_{\mathrm{preamp}}}{Z_a + Z_{\mathrm{preamp}}} \\ P_{\mathrm{out}} &= \frac{(U_{\mathrm{preamp}} G_{\mathrm{rec}} L_{\mathrm{line}})^2}{Z_L} \end{aligned} \tag{2}$$

The power of the noise from the lander (black lines in Fig. 8) was recorded during the lander EMC test. The red lines in Figure 8 represent the lander noise after EMI mitigation. The position of the red line relative to the position of the yellow line could be used to analyse detectability of solar burst. Figure 8 shows that after EMI mitigation the solar burst with average flux density could be detected by the LFRS in some frequency range such as $1-6$ MHz, while solar burst with peak flux density could be detected by the LFRS in the entire working frequency range of $0.1-40$ MHz. In other words, when the radiation flux density of solar burst events or other similar events reach higher than 10^{-18} W m^{-2} Hz^{-1}, these events might be detected by the LFRS.

5 CONCLUSIONS

The properties, ground experiments and performance evaluation of the LFRS are briefly described in this paper. The results of the ground experiments show that the method using 20 cm long antenna as reference antenna for EMI mitigation is helpful. The noise from the lander can by reduced by 20 dB to 40 dB, while the signals are not severely distorted in the frequency range of $0.1-40$ MHz with the above method. The detection capability and performance analysis show that after EMI mitigation solar burst with average flux density could be detected by the LFRS in some frequency ranges such as $1-6$ MHz, while the solar burst with peak flux density could be detected by the LFRS in the entire working frequency range of $0.1-40$ MHz. However, a lot of work needs to be done in the future lunar surface detection. Because of the difference between the experimental environment and the real environment of the lunar surface, there may be a better way for EMI mitigation. Some suggestions to improve the EMI mitigation: after a period of observation on the lunar surface, the characteristics of the lander noise should be carefully studied. A more accurate model of the lander noise will be very helpful for the process and analysis of the spectra collected by the LFRS. Furthermore, more advanced and complicated algorithms

can be tried to improve the detection capability of the LFRS (Fridman & Baan 2001).

Acknowledgements This work was funded by the Youth Innovation Promotion Association of Chinese Academy of Sciences (CAS)(Grant No. 2015334) and the National Natural Science Foundation of China (Grant No. 11941002). The authors thank the Ground Application System of Lunar Exploration, National Astronomical Observatories and Institute of Electronics, CAS, for their valuable and efficient assistance with providing the data and data calibration.

References

Arts, M., Wal, E. V. D., & Boonstra, A. J. 2010, in ESA Antenna Workshop on Antennas for Space Applications, ed. H. Lacoste, Vol. 32 (Noordwijk: ESA), 5

Bentum, M. J., Boonstra, A. J., & Baan, W. 2011, in General Assembly and Scientific Symposium (Piscataway: IEEE), 1

Boonstra, A. J., Saks, N., Bentum, M. J., Klooster, V. T. K., & Falcke, H. 2010, in Cospar Scientific Assembly (Paris: COSPAR), 11

Fridman, P. A., & Baan, W. A. 2001, Journal of Astronomy and Astrophysics, 378, 327

Jester, S., & Falcke, H. 2009, New Astronomy Reviews, 53, 1

Ji, Y., Zhao, B., Fang, G., et al. 2017, Journal of Deep Space Exploration, 4, 150

Lazio, T. J. W., Macdowall, R. J., Burns, J. O., et al. 2011, Advances in Space Research, 48, 1942

Li, C., Wang, C., Wei, Y., & Lin, Y. 2019, Science, 365, 238

Takahashi, Y. D. 2003, Advances in Space Research, 31, 2473

Wolt, M. K., Aminaei, A., Zarka, P., et al. 2012, Planetary and Space Science, 74, 167

Wu, W., Wang, Q., Tang, Y., et al. 2017, Journal of Deep Space Exploration, 4, 111

Wu, W., Li, C., Zuo, W., et al. 2019, Nature Geoscience, 12, 222

Zarka, P., Bougeret, J. L., Briand, C., et al. 2012, Planetary and Space Science, 74, 156